Influence of mantle dynamics on the topographic evolution of the Tibetan Plateau: Results from numerical modeling

Ivone Jiménez-Munt[1] and John P. Platt[2]

Received 6 March 2006; revised 9 August 2006; accepted 11 September 2006; published 11 November 2006.

[1] We investigate numerically the evolution of crustal and lithospheric thickness, thermal structure, topography, and strain rate of the Tibetan Plateau through time, using the thin viscous sheet approach. We show that lithospheric mantle must have been removed from beneath Tibet to explain the present surface elevation and lack of regional surface slope. In the absence of this removal, the modeled topography reaches a maximum elevation of <4000 m (for weak rheology), or the surface slopes significantly northward (for strong rheology). The crust must have been warmed and weakened by an increase of radiogenic heat production at depth due to crustal thickening. In the absence of this warming, viscous stresses associated with plate convergence exceed stresses produced by topography, and the present pattern of vertical thinning and east-west extension would not have developed. Continuous removal of lithosphere, by delamination or convection, does not allow sufficient crustal warming and fails to reproduce either the present topography or the pattern of active deformation on the plateau in a reasonable time. Geologically rapid removal of the lithospheric root beneath the thickened crust of Tibet successfully explains the current elevation of the plateau, its lack of surface slope, the steep south and north margins, and the pattern of the present deformation, including vertical thinning, E-W extension, and extrusion and vertical axis rotation on the eastern margin. Our modeling suggests that this removal took place within the last 12 m.y. **Citation:** Jiménez-Munt, I., and J. P. Platt (2006), Influence of mantle dynamics on the topographic evolution of the Tibetan Plateau: Results from numerical modeling, *Tectonics*, *25*, TC6002, doi:10.1029/2006TC001963.

1. Introduction

[2] The Himalayan-Tibetan orogen is the largest collisional system on our planet, and represents a large-scale natural experiment in the contractional deformation of continental lithosphere. It is also the largest active example of extensional tectonics in a zone of continental collision. As a result it has attracted a lot of attention from both observational and theoretical geodynamicists, and a rapidly increasing amount of geological and geophysical data has become available. Many attempts have been made to model the mechanics of deformation of the India-Asia collision zone, emphasizing either its history or its present dynamical state, and none of these attempts have won universal acceptance. Numerous causes of the Tibetan extension have been proposed: gravitational collapse driven by excess gravitational potential energy arising from the buoyant crustal root and the upwelled asthenosphere [*Chen and Molnar*, 1983; *Dewey et al.*, 1988]; vertical variations of lithospheric rheology and stress states [*Bird*, 1991; *Shen et al.*, 2001]; boundary conditions, such as oblique convergence or basal shear associated with subduction of the Indian plateau or tectonic boundary conditions in eastern Asia [*Yin*, 2000; *Liu and Yang*, 2003]. Debate continues about even the most fundamental aspects of the structure and mechanical state of this system.

[3] One of the most successful approaches to modeling the India-Asia collision was also one of the earliest and simplest: the thin viscous sheet approach [e.g., *Houseman and England*, 1986; *England and Houseman*, 1986]. Its success was because it only attempts to explain the largest-scale features of the system: those that are at a scale larger than any of the mechanical heterogeneities and discontinuities that complicate its behavior, including the crust. Hence it is easy to test the model results against the first-order features of the collision zone. The model failed, however, to explain the present elevation of the Tibetan Plateau or the widespread normal faulting without appealing to an external process to increase the overall buoyancy of the thickened lithosphere. This was justified in terms of the development of Rayleigh-Taylor instabilities in the lower part of the thermal boundary layer [*Houseman et al.*, 1981; *England and Houseman*, 1989], a concept already developed to explain the thermal evolution of oceanic lithosphere [*Parsons and McKenzie*, 1978]. This concept has been widely debated, and more recent modeling approaches have not explicitly addressed questions about the evolution of crustal and lithospheric thickness and of surface elevation in the Tibetan Plateau.

[4] Our interest in this paper is therefore to investigate these questions in more detail, using the thin viscous sheet approach in a significantly more advanced form that takes account of thermally induced changes in the bulk rheology. We model the deformation of a rheologically stratified

[1]Group of Dynamics of the Lithosphere, Institute of Earth Sciences "Jaume Almera," Consejo Superior de Investigaciones Científicas, Barcelona, Spain.
[2]Department of Earth Sciences, University of Southern California, Los Angeles, California, USA.

0278-7407/06/2006TC001963

lithosphere, for which the coupled system of equations for momentum and energy conservation is solved numerically. We examine the way the crustal and lithospheric thickness evolve in three dimensions during the progressive indentation of India, with and without removal of the lower lithosphere, and how these processes affect the evolution of topography, thermal structure, and tectonic style. The aim of this work is not to reproduce precisely the present shape of the Tibetan Plateau, but to study the role of the lithospheric mantle and asthenosphere, and the related thermal distribution, on the uplift of the plateau.

2. Geological and Geophysical Constraints

[5] The crust that now forms the main part of the Tibetan Plateau is an amalgam of displaced continental terranes and slices of oceanic crust and sediment that were assembled by accretion and collision during the Mesozoic [*Dewey et al.*, 1988]. These processes are likely to have formed crust of variable thickness and elevation [*Murphy et al.*, 1997], and there is evidence that parts of the southern margin of Tibet (the Gangdese batholith in the Lhasa terrane) were significantly elevated prior to India-Asia collision [*England and Searle*, 1986], perhaps forming an active convergent margin analogous to the present-day Andes. Scattered remnants of marine sedimentary rocks of Cretaceous age [*Yin and Harrison*, 2000] suggest, however, that by the late Mesozoic much of the surface of Tibet lay close to sea level. Given its likely structure and composition this implies an overall crustal thickness in the range 25–35 km, and it is unlikely to have had a well-developed lower crustal layer comparable to that found beneath continental cratons.

[6] The present thickness and elevation of the Himalayan orogen and the Tibetan Plateau are generally attributed to the collision and subsequent convergence of India with Asia, starting at around 50–54 Ma [*Searle et al.*, 1987]. The postcollisional evolution of the plateau is highly uncertain, however, partly because of the lack of age control on syntectonic to posttectonic continental sediments, and partly because of the difficulty of constraining paleoelevations. Hence the main constraints on the way the plateau formed have to come from its present-day structure and kinematics.

[7] The most clear-cut feature of the Tibetan Plateau is the pattern of elevation (Figure 1a). Although parts of the plateau interior show considerable relief (up to 3000 m), the average elevation is close to 5000 m, with no overall topographic gradient [*Molnar and Lyon-Caen*, 1989; *Fielding et al.*, 1994] and with steep topographic gradients across the southern and northern plateau margins. The geomorphic plateau extends south of the Indus-Tsangpo suture, which marks the line of collision between India and Asia, and incorporates the Tethyan Himalaya, which comprises largely unmetamorphosed thrust sheets derived from the distal northern margin of India [*Hodges*, 2000]. In terms of average elevation there is no rim on the southern margin of the plateau: the great peaks of the High Himalaya are offset by correspondingly deep valleys, so that the average elevation is similar to the rest of the plateau. The southern margin of the plateau is therefore defined by the steep southern slope of the Himalaya. Gradients on the northern margin of Tibet, where it is defined by the Altyn Tagh fault, are also steep, but they are much more gentle on the west, northeast, and east sides of the plateau, with the exception of the Longmen Shan, where the plateau drops off steeply into the Szechuan Basin. Viewed on a larger scale, the high topography of Tibet can be seen as diminishing gradually for several thousand km north across central Asia, with interruptions such as the Tarim Basin where the local lithospheric strength may have been sufficient to resist contractional deformation [*Neil and Houseman*, 1997].

[8] The crustal thickness beneath Tibet is not well defined, but appears to decrease from around 70 km in the south to about 65 km in the north, where there is a correspondingly greater thickness of relatively low-density Paleozoic sediment in the upper crust [*Haines et al.*, 2003]. The mechanism(s) by which the crust achieved this great thickness is one of the central areas of debate at present. The upper mantle structure is even less well defined. Available evidence on seismic velocities suggests that lithospheric mantle beneath much of northern Tibet is relatively thin and warm [*McNamara et al.*, 1997], although this has been disputed on the basis of surface wave analysis [*Griot et al.*, 1998; *Tapponnier et al.*, 2001]. The results of the INDEPTH II profile suggests that cold Indian lithosphere may be underthrust horizontally beneath southern Tibet and the Lhasa block, perhaps as far as the Bangong suture [*Hauck et al.*, 1998]. At present rates of convergence along the Himalayas (about 22 km m.y.$^{-1}$) this underthrusting of Indian lithosphere may have taken place during the last 12 m.y.

[9] Tomographic inversion of P wave velocities measured along the INDEPTH III survey north of the Bangong suture indicates significant velocity heterogeneity in the upper mantle down to 300 km, with steeply dipping bodies of seismically fast material beneath central Tibet, and seismically slow material at shallow levels beneath the southern and northern parts of the plateau [*Tilmann et al.*, 2003]. The presence of large-scale structure in the upper mantle is also borne out by receiver function analysis, which has identified surfaces of impedance contrast dipping in various directions within the upper mantle [*Shi et al.*, 2004]. These structures have been interpreted as subducting Indian lithosphere [*Tilmann et al.*, 2003], delaminated lithospheric mantle [*Shi et al.*, 2004], or convective downwellings in the lower part of a thickened thermal boundary layer [*Houseman and Molnar*, 2001]. To some extent these differing interpretations simply reflect different perceptions

Figure 1. (a) Topography and S-N cross section of the topography; (b) tectonic map, color shades show elevation (1000, 3000, and 5000 m contours). ATF, Altyn Tagh Fault; MBT, Main Boundary Thrust of Himalaya; JF, Jiali Fault Zone; KF, Karakorum Fault; ITS, Indus-Tsangpo Suture; BNS, Bangong-Nujiang Suture; (c) topography and horizontal surface velocity (GPS data [*Wang et al.*, 2001]).

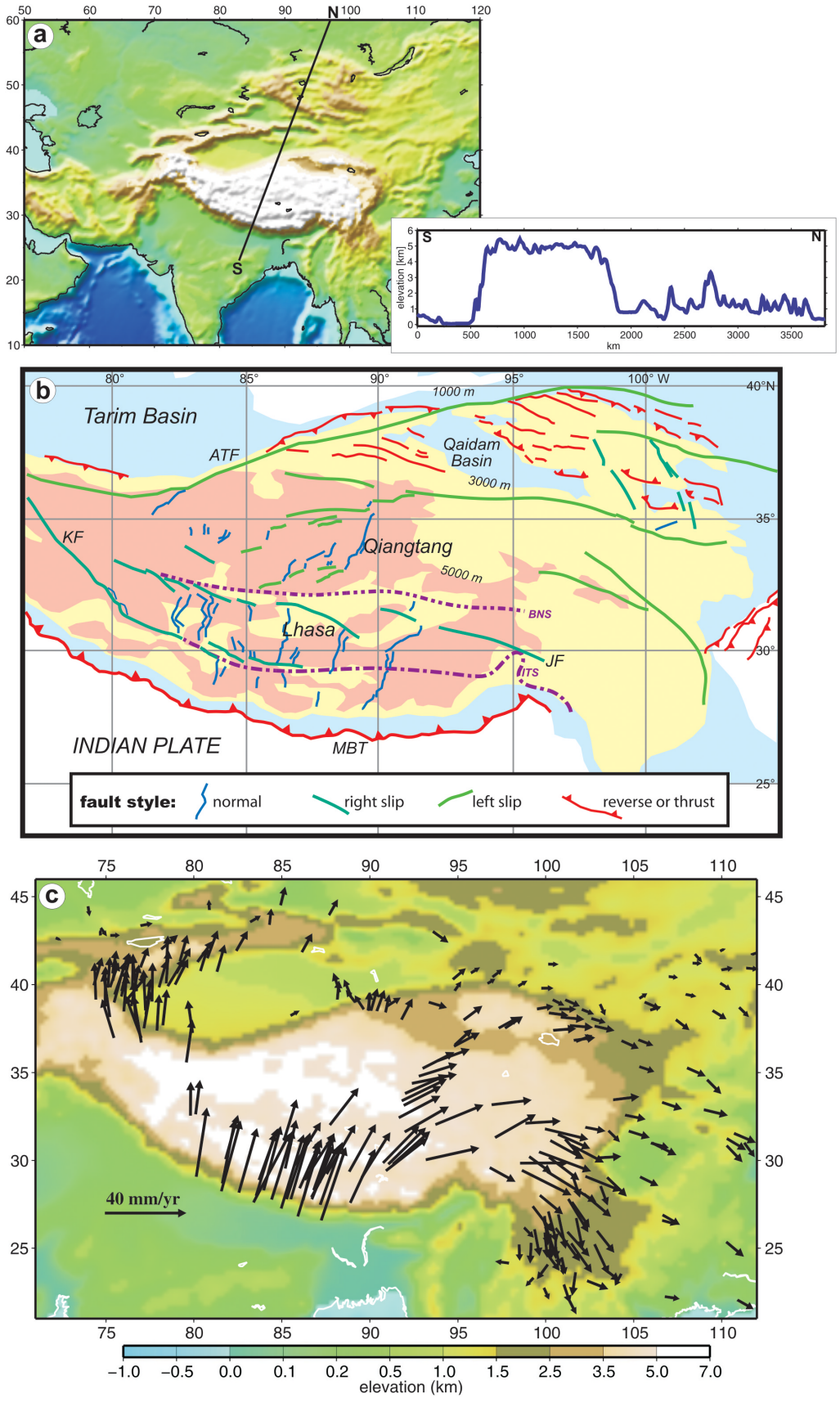
a
N
S
elevation [km]
km
b
Tarim Basin
ATF
Qaidam Basin
1000 m
3000 m
KF
Qiangtang
5000 m
BNS
Lhasa
JF
ITS
INDIAN PLATE
MBT
fault style:
normal
right slip
left slip
reverse or thrust
c
40 mm/yr
elevation (km)

Figure 1

about the mechanical state of the lithospheric mantle beneath Tibet. What they all have in common is the idea of some sort of circulation of material in the uppermost mantle driven by thermally induced density contrasts.

[10] Temperatures within the Tibetan crust are relatively high, as indicated, for example, by the depth to the α-β quartz transition, which suggests a temperature of 700°C at 18 km depth beneath central Tibet [*Mechie et al.*, 2004]. Given the exceptional thickness of the crust and its likely high radiogenic heat generation, the mantle contribution to the overall thermal budget is unclear. Evidence for anomalously warm mantle beneath the plateau comes from the young magmatic history, which includes K-rich magmatism of Miocene to Recent age [*Turner et al.*, 1996; *Williams et al.*, 2001]. This suggests partial melting of lithospheric mantle, which *Turner et al.* [1996] interpret as indicating the convective removal and sinking of thickened lithosphere. Bright spots in the INDEPTH II seismic reflection line have been interpreted as zones of partial melt at about 20 km depth within the Tibetan continental crust [*Alsdorf et al.*, 1998]. Adakitic volcanism of mid-Tertiary to late Miocene age in southern Tibet is interpreted to indicate lower crust melting [*Chung et al.*, 2003]. *Hou et al.* [2004] report the occurrence of potassic adakites from south Tibet; and they conclude that the melting of the thickened lower crust in south Tibet requires a significant thermal anomaly, which was most likely triggered by mantle-derived ultrapotassic magmatism formed by removal of subcontinental lithospheric mantle or breakoff of a subducted continental slab during the late Miocene.

[11] Late Miocene to Recent deformational features on the plateau are dominated by a linked pattern of strike-slip and normal faults [*Taylor et al.*, 2003] that act together to produce E-W extension, N-S shortening, and vertical thinning. The normal faults trend predominantly N-S, and they are linked by strike-slip faults trend ENE (left-slip) and ESE (right-slip), which at least in part act as transfer structures. Some graben are oblique to the main N-S trend, particularly in western Tibet, but these appear to be transtensional structures, and do not indicate significant deviations in the overall pattern of E-W extension [cf. *Kapp and Guynn*, 2004].

[12] The seismicity of the plateau confirms the evidence from young fault traces on the plateau: the dominant modes of deformation are strike-slip and normal faulting [*Molnar and Lyon-Caen*, 1989]. Strike-slip focal mechanisms indicate N-S shortening and E-W extension in the western part of the plateau, swinging through NE-SW shortening to E-W shortening and N-S extension on the eastern margin. Normal fault mechanisms indicate a more consistent pattern of E-W to ESE-WNW extension. One of the most striking aspects of the seismicity is the strong correlation between the mode of faulting and the surface elevation. Reverse faulting is confined to regions on the margins of the plateau, in the Himalaya, the Nan Shan, and the Longmen Shan, with surface elevations less than 3000 m; normal fault mechanisms are confined to the high plateau where elevations exceed 4000 m [*Molnar and Lyon-Caen*, 1989; *Molnar et al.*, 1993]. This pattern strongly suggests that buoyancy forces associated with topography exert a strong control over the present-day pattern of deformation.

[13] Although coverage is limited, GPS data across the Tibetan Plateau reveal a very clear and coherent kinematic pattern (Figure 1c) [*Wang et al.*, 2001]. Northward velocity relative to Asia decreases steadily across the plateau, with the steepest gradients in the south, where at least 14 mm yr^{-1} of northward motion is accommodated within the 300 km wide Himalayan thrust belt, giving a gradient of >0.047 mm yr^{-1} km^{-1}. Across the main body of the plateau in central and eastern Tibet northward velocity decreases steadily to zero at the northern margin, giving an overall gradient of ~0.016 mm yr^{-1} km^{-1}. This decrease in north velocity is accompanied by an increase in east velocity, so that the vectors swing clockwise. East velocity reaches a maximum of around 16 mm yr^{-1} in east-central Tibet, but decreases both northward and eastward, as relative motion is accommodated in the thrust belts to the north and east of the plateau. Farther west there is less data, but the measurements suggest a simple pattern of decreasing north velocity across the plateau without much change in the overall orientation of the velocity vectors.

3. Topics of Debate Concerning the Formation of the Tibetan Plateau

3.1. When and by What Mechanism Did the Crust and the Lithosphere Reach Their Present Thicknesses?

[14] The INDEPTH seismic profiles suggest that underthrusting of Indian crust is limited to southern Tibet, so that the bulk of the plateau has formed by thickening of Asian crust. This conclusion is supported by the paleomagnetic data, which indicate that the crust of southern Tibet has moved north by about 1900 km since collision [*Achache et al.*, 1984]. It seems probable that crustal thickening proceeded gradually from south to north, but few surface structures have been confidently identified as being related to thickening, so constraints on the timing and amount of strain involved are lacking. A major area of disagreement, however, concerns the mechanical behavior of the Asian continental lithosphere during thickening. One end-member approach has been to treat the lithosphere as a viscous fluid, which thickened in front of the indenting Indian plate, and flowed away from the indentor under the gravitational forces associated with its high topography [e.g., *England and Houseman*, 1986]. The other end-member approach is to consider Tibet to have formed by the progressive subduction and accretion of continental microplates [*Tapponnier et al.*, 2001; *Replumaz and Tapponnier*, 2003]. The crust in this approach is treated as a series of accretionary wedges, beneath which the mantle lithosphere was subducted in plate-like fashion.

[15] A related issue concerns the fate of the mantle lithosphere that underlay the Asian crust prior to thickening. Given that the crust is probably around twice its precollisional thickness, we should expect on average around 180 km thickness of mantle lithosphere to have accumulated beneath it. Much of this material has disappeared. In a modification of

the original thin viscous sheet approach, *England and Houseman* [1989] suggested that the lower part of the lithospheric mantle was removed by convective downwelling at some time after the main phase of thickening beneath the plateau. *Tapponnier et al.* [2001], on the other hand, suggests that the lithospheric mantle was removed continuously by delamination during the thickening process. These two hypotheses have very different implications for the mechanical evolution of the plateau, as well as the history of its surface elevation (see below).

3.2. When and by What Intervening Stages Did the Plateau Achieve Its Present Surface Elevation?

[16] The exceptionally high elevation of the plateau, and the lack of significant elevation gradients within it, demand a straightforward mechanical explanation. *England and Houseman* [1986] suggested that the present elevation of the plateau represents an equilibrium between its tendency to thicken as a result of the northward motion of India, and to its tendency to extend and thin under the gravitational forces created by its high elevation. This explanation runs into two problems, however. Given normal mantle and crustal densities, a simple doubling of the thickness of continental lithosphere should produce a surface elevation of around 3000 m, much less than that of Tibet. Secondly, this explanation would predict a pattern of deformation in the plateau involving predominantly strike-slip faulting, with increasing amounts of thrust faulting at the margins, rather than the widespread normal faulting that is indicated by both the surface morphology and the seismicity. *England and Houseman* [1989] therefore suggested that widespread convective removal of lithospheric mantle had occurred beneath the whole plateau at a late stage in its evolution, resulting in an isostatic increase of elevation by around 2000 m to around its present value. The resulting buoyancy forces outweighed the compressional forces associated with plate convergence, so that the plateau began to extend and thin. *Molnar et al.* [1993] suggested that convective removal occurred rapidly beneath the whole plateau at about 8 Ma, and related this event to the initiation of buckling instabilities within the oceanic lithosphere of the Indian plate, and to climatic changes in the late Miocene.

[17] The elevation history of the plateau reflects the history of lithospheric thickening and removal, by whatever mechanism, of lithospheric mantle. If, as suggested by *Tapponnier et al.* [2001], lithospheric removal occurred continuously or episodically during crustal thickening, then the increase in surface elevation should have been fairly continuous as well. Determination of paleoelevations is difficult and inaccurate, however, and different lines of evidence lead to very different conclusions. *Rowley and Currie* [2006] suggest on the basis of oxygen isotope data in soils that much of Tibet may have been at high elevation by 39 Ma, *Spicer et al.* [2003] used leaf morphology to suggest that southern Tibet was close to its present elevation by 15 Ma, whereas *Wang et al.* [2006] used the carbon isotope composition of mammalian teeth to infer significant surface uplift in southern Tibet as recently as 7 Ma. The onset of normal faulting in the N-S trending graben in southern Tibet, and the emplacement of N-S dikes, have been dated at around 13–18 Ma [*Coleman and Hodges*, 1995; *Blisniuk et al.*, 2001; *Williams et al.*, 2001], and this is widely regarded as indicating a significant increase in surface elevation and a corresponding change in the regional stress field in mid-Miocene time. *Clark et al.* [2005] point to an increase in incision rates, and therefore of elevation, in eastern Tibet at 13 Ma, and detailed magnetostratigraphic studies of molasse deposits along the Altyn Tagh Fault by *Sun et al.* [2005] show that the accumulation of coarse conglomerate began at 13.7 Ma, and they attribute this to the uplift along the northern edge of the Tibetan Plateau, a process that continued until at least 9 Ma. On the basis of the timing of alkalic magmatism, however, *Chung et al.* [1998] suggest a diachronous uplift history for the Tibetan Plateau, with convective removal of the lower lithosphere inducing rapid uplift in the east beginning at around 40 Ma and in the west about 20 m.y. later. Clearly the evidence at present is insufficient to distinguish among the various model-based predictions.

3.3. How Can We Explain the Present-Day Deformation of the Plateau in Terms of N-S India-Asia Convergence?

[18] The divergences of opinion about the present-day pattern of deformation in Tibet resemble those about its history, and reflect the same differences in philosophy. At one extreme there is the viewpoint reflected by *Avouac and Tapponnier* [1993], who consider the Tibetan crust to consist of an array of small, internally rigid, lithospheric blocks, which accommodate India's northward motion by strike-slip motion along their boundaries, and in the process escape eastward. Deformation is effectively assumed to be horizontal plane strain, and this approach is nicely illustrated by the plane strain analogue experiments published by *Molnar and Tapponnier* [1977]. Normal faulting on the plateau is assumed to be an incidental side effect of the incompatibilities between the blocks.

[19] The other end-member in the spectrum is the thin viscous sheet approach described in the previous section. Present-day deformation of the plateau is treated as the reflecting N-S shortening imposed by the northward motion of India and vertical shortening resulting from buoyancy forces, resulting in an overall deformation lying in the constrictional field with E-W maximum rate of extension [*England and Houseman*, 1989].

[20] A third approach reflects the likely rheological layering of the Tibetan lithosphere, with a very weak, possibly partly molten, middle or lower crust [*Clark and Royden*, 2000; *Shen et al.*, 2001]. They suggest that the present-day surface deformation results from flow of the weak lower crust beneath a thick constant viscosity upper crust under gravitational body forces. They specify velocity at the Moho and impose that the lithospheric mantle beneath Tibet has plate-like behavior, assuming that all deformation is localized along the mantle suture, and is undergoing some form of subduction. They calculate the topography assuming crustal Airy compensation, without taking into account the possible interaction between the lithospheric mantle and asthenosphere. A variant on this theme is the channel flow

concept of *Beaumont et al.* [2001], here the upper crust is assumed to be strong and rigid, the lower crust and lithospheric mantle are assumed to be plate-like, and the middle crust is treated as a fluid that is being extruded southward, emerging in the Himalaya as the High Himalayan crystallines.

[21] The emphasis in this paper is on the way the lithospheric mantle and the thermal structure of the lithosphere have controlled the distribution and evolution of crustal thickness, topography, and strain rate of the Tibetan Plateau through time. We seek in particular a mechanically consistent explanation as to how the plateau has reached its present state from its likely starting configuration.

4. The Model

[22] We use a finite difference numerical model of lithospheric deformation (code called Uhuru), where we adopt a thin viscous sheet approach with vertically averaged viscosity. This approach assumes local isostasy of the whole lithosphere and vertical integration of the lithospheric strength to reduce the three-dimensional problem to a planform model, where the horizontal velocity components do not change with depth, and temperature is calculated in one dimension [*Houseman and England*, 1986; *Bird*, 1989]. Local isostatic equilibrium is an acceptable approximation, as gravity anomalies show that over length scales of a few hundreds kilometers, density contrasts within the lithosphere are isostatically compensated [*England and Molnar*, 1997]. Furthermore, the gravity field in Tibet indicates that the topography there is for the most part in local isostatic compensation [*Jin et al.*, 1994]. The horizontal velocity field includes the effects of lateral variations of gravitational potential energy related to crustal and lithospheric thickness variations [*Jiménez-Munt et al.*, 2001, 2005a]. The reader is referred to *Jiménez-Munt et al.* [2005a] for detailed explanations about the modeling techniques and assumptions.

[23] The thin viscous sheet approach is not suited to describing processes at the scale of a thrust belt such as the Himalayas, nor can it predict the location and behavior of individual strike-slip faults, such as the Altyn Tagh, Karakoram, or Red River fault. It can however, predict in what parts of the system strike-slip faulting, as opposed to reverse or normal faulting, is likely.

[24] Complete decoupling of crust from lithosphere, or upper crust from lower crust, as proposed by *Clark and Royden* [2000] or *Beaumont et al.* [2001], for example, clearly invalidates the thin viscous sheet approach, or for that matter any attempt to describe the deformation of the lithosphere as a single mechanical entity. While we accept that the degree of crust-mantle coupling remains an open question, we think that at the scale of Tibet it is likely that the lithosphere as a whole is controlling the pattern of deformation, and we wish to explore this concept further. We are impressed by the evidence from seismic anisotropy analysis that the deformation of the mantle lithosphere below Tibet closely resembles the pattern of surface flow revealed by geodetic studies [*Holt et al.*, 2000].

[25] The thin viscous sheet approach allows us to investigate in a straightforward way variations in the thermal structure, bulk rheology, density, surface elevation, and gravitational potential energy on the flow field, and to compare the predictions against observations. Because only bulk properties are considered, the number of variables is limited, and hence exploration of parameter space is relatively easy. The same technique has been successfully used to investigate the mechanisms leading to the postcollisional tectonic evolution and the different roles of gravitational and tectonic forces on the present-day stress of the Alps [*Jiménez-Munt et al.*, 2005b].

4.1. Convective Removal of Lithosphere

[26] The mutual interactions among viscous lithospheric deformation and thermal advection and conduction in the lithosphere are accounted for in this fully coupled thermomechanical model. The temperature distribution is calculated in each time step, which in turn determines the thermal lithospheric thickness and the topography using a local isostasy approach.

[27] We also consider the effect of the removal of lithospheric mantle on the evolution of the continental collision zone. We study both continuous removal (as in a subduction zone) and the instantaneous detachment of the lower part of the lithospheric mantle at a late stage in the evolution of the collision zone, as described by *England and Houseman* [1989] and *Platt and England* [1994], for example. Figure 2 shows an example of the evolution of the geotherm before and after the removal of lithospheric mantle. In this one-dimensional (1-D) model, we impose thickening at a constant rate of 4×10^{-16} s^{-1} for 50 m.y., with lithospheric mantle removal at 40 m.y. Almost the entire lithospheric mantle is removed and replaced by asthenospheric mantle. This is an instantaneous process in which the lithosphere loses mantle component. Under these conditions, the elimination of $\sim$140 km of lithospheric mantle causes an increase of the Moho temperature by 300°C 10 m.y. after the removal, and a decrease of the average density ($\sim$20 kg m^{-3}) of the $\sim$35 km of new lithospheric mantle created in 10 m.y. after removal by conduction and lithospheric thickening; note that the constant thickening-rate of 4×10^{-16} s^{-1} is still imposed after the lithospheric mantle removal. This decrease in density, together with the replacement of part of the lithosphere by the lighter asthenospheric mantle, results in an uplift of the surface by $\sim$2 km. Hence the removal of the lithosphere root results in an increase in the gravitational potential energy (GPE) or equivalently the depth-averaged vertical stress ($\overline{\sigma}_{zz}$):

$$\overline{\sigma}_{zz}(x,y) = \frac{1}{La}\int_0^{La} \sigma_{zz}(x,y,z)dz = \frac{1}{La}\int_0^{La}\left(\int_{\substack{\text{surface}\\(z<0)}}^{z} g\rho(x,y,z)dz\right)dz = \frac{\text{GPE}}{La}, \tag{1}$$

where La is the thickness of the plate (depth of compensation in the asthenosphere, usually 300 km, plus the surface

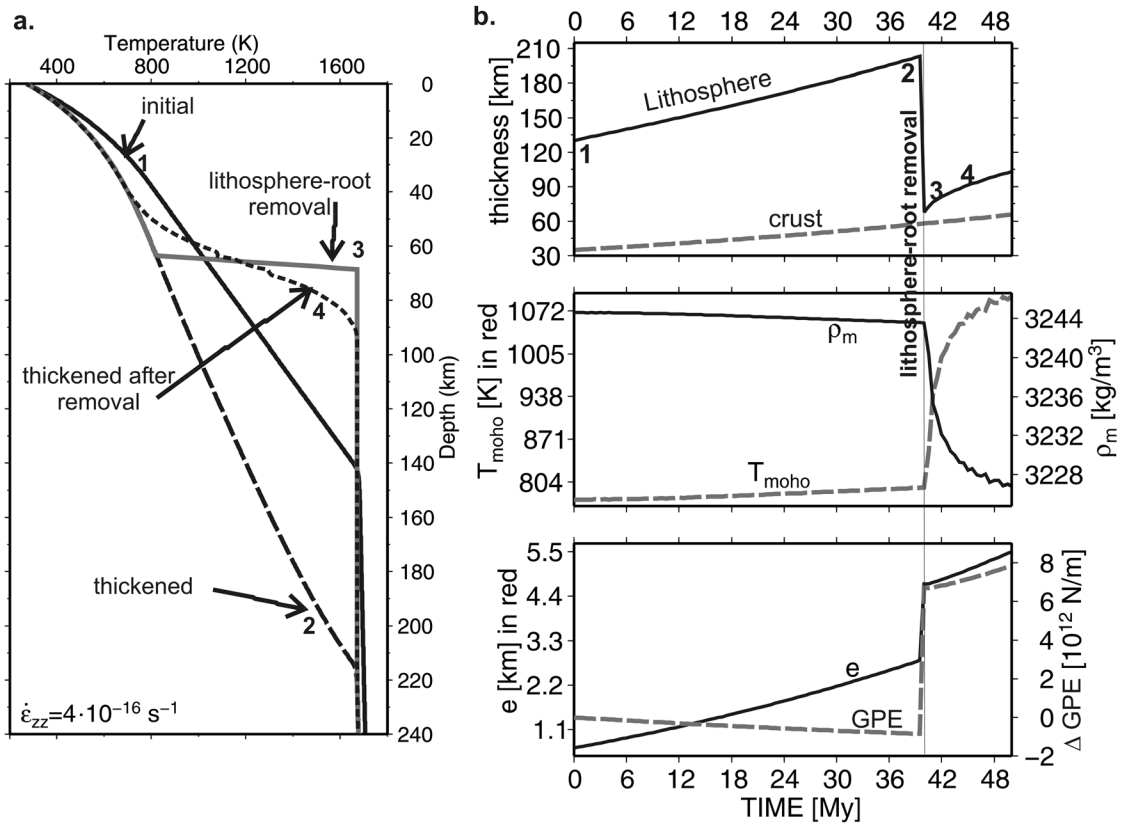

Figure 2. (a) Time evolution of a geotherm under constant thickening ($\dot{\varepsilon}_{zz}$ = 4. × 10^{-16} s^{-1}) and at different stages: curve 1, initial; curve 2, after 40 m.y. of constant thickening; curve 3, after removal of the lithospheric mantle; and curve 4, 2 m.y. after the lithospheric removal, resulting from conduction and constant thickening. (b) Time evolution of: lithosphere and crustal thickness; Moho temperature and lithospheric mantle density; elevation and changes in gravitational potential energy (ΔGPE = GPE(t)–GPE(t = 0)).

elevation), ρ is the density on each layer, and g is the acceleration due to gravity (9.8 m s^{-2}). Figure 2 also shows how the GPE changes with time, decreasing first with the thickening of crust and lithosphere, and then a large increase of 7.5 10^{12} N m^{-1} after the removal of the lithospheric root. Note that from 0 to 40 m.y. GPE decreases because crust and lithospheric mantle have a similar thickening rate; when we assume a continuous convective removal of the lithospheric root GPE could increase with thickening.

[28] These changes in $\overline{\sigma}_{zz}$ or GPE can have a major role on the thin sheet calculation. Lateral variation of the GPE could result in some thinning of the plateau even in an area where the regional tectonic regime is highly compressional. The equations governing the lithosphere deformation in the thin sheet approach are the horizontal components of the equilibrium equation (see *Jiménez-Munt et al.* [2001, 2005a] for more details),

$$\frac{\partial}{\partial x_j}\left[\eta\left(\frac{\partial u_i}{\partial x_j}+\frac{\partial u_j}{\partial x_i}\right)\right]+\frac{\partial}{\partial x_i}\left[2\eta\left(\frac{\partial u_1}{\partial x_1}+\frac{\partial u_2}{\partial x_2}\right)\right]=\frac{\partial \overline{\sigma}_{zz}}{\partial x_i} \quad i,j=1,2.$$

where u_1 and u_2 are the horizontal components of the velocity on the x_1 and x_2 directions, and η is the effective viscosity (depth-averaged) of the plate; and the lateral changes of $\overline{\sigma}_{zz}$ are related to changes of crustal and lithospheric thicknesses and densities (equation (1)).

4.2. Model Setup

[29] To save computing time, we model only the right half of the symmetric solution (Figure 3a), which corresponds to the eastern half of the Tibetan Plateau. The horizontal dimensions of the modeled domain are 4000 km from west to east and 6000 km from south to north, with horizontal grid spacing of 35 km. At the end of the deformation history this domain corresponds to the region between 14°N to 68°N and 85°E to 127°E. The Indian lithosphere has practically no internal deformation; we treat it as a nearly rigid block with a viscosity of 10^{25} Pa s, moving to the north with a long-term average convergence rate of 50 mm yr^{-1} (Figure 3a). North and east boundaries are fixed at zero velocity; and the western boundary is free slip (u_1 = 0 and τ_{12} = 0, zero normal velocity and deviatoric shear stress) to preserve the symmetry of the model.

[30] For simplicity, we have assumed initially uniform crustal and lithospheric thicknesses. A representative value of 35 km for the crustal thickness has been assumed on the

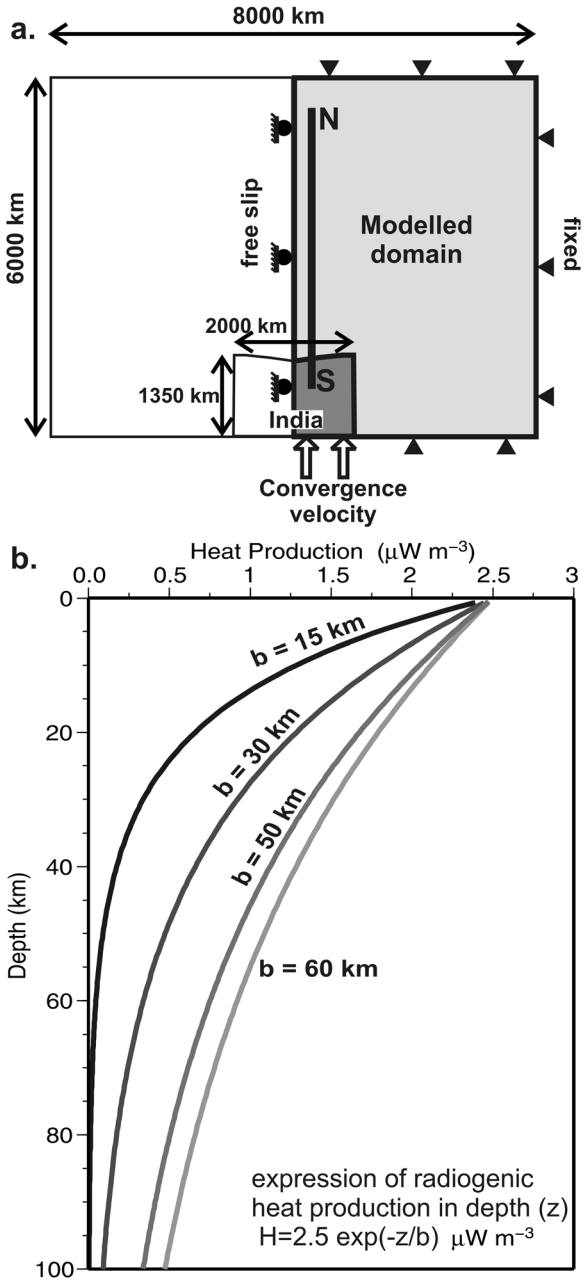

Figure 3. (a) Model setup and boundary conditions. For computing time, we just model the right half of the symmetric solution (gray domain). The horizontal dimensions are 4000 km from east to west and 6000 km from north to south, with a grid space of 35 × 35 km. India is assumed as a rigid block with a viscosity of 1×10^{25} Pa s and dimensions 1000 × 1350 km. The initial crustal and lithospheric thicknesses are 35 and 130 km, respectively, resulting in an elevation of 580 m. (b) Radiogenic heat production with depth for different b coefficients.

basis of the present-day crustal thickness in the undeformed zones, such as India and north Eurasia [*Bassin et al.*, 2000]. The value of 130 km adopted for the lithospheric thickness, together with the assumption of local isostasy and the parameters listed in Table 1, results in an elevation of 580 m.

[31] One of the most influential rock properties on temperature distribution at lithospheric scale is the heat production associated with natural radioactive decay, which amounts to about 40% of the total heat released to the atmosphere by the continental lithosphere. Volumetric heat production measurements range between 1 and 4 μW m^{-3} for upper crustal rocks, 0.1 and 1 μW m^{-3} for lower crustal rocks, and 0 and 0.02 μW m^{-3} for mantle rocks [*Wollenberg and Smith*, 1987]. In this work we assume an exponential decrease with depth z of radiogenic heat production within the crust as $H = H_o \exp(-z/b)$. We use a mean value for continental crust where the heat production at the surface is $H_o = 2.5$ μW m^{-3} and the decay exponent $b = 15$ km. However, much of the high plateau of Tibet is underlain by crust that was formed by thrust stacking both before and during collision, and is therefore likely to have higher values of heat production at depth. To simulate this, for crust thicker than 40 km we increase b to 55 km. Figure 3b shows the distribution of radiogenic heat production with depth for different values of the decay exponent. For $b = 15$ km the crustal radiogenic heat production below 40 km is less than 0.2 μW m^{-3}. For $b = 55$ km, the heat production at 40 km depth is $\sim$1.2 μW m^{-3}, which is the average value for middle crust rocks.

5. Results and Discussion

[32] We perform several models to study the effect on the long-term deformation of the rheology of the lithosphere and the crustal heat production. Our first attempt was to try to simulate the Tibetan Plateau without considering any kind of removal of the lithosphere root. We were particularly interested in whether we could produce a plateau and a pattern of deformation comparable to present-day Tibet without invoking lithospheric removal. We ran the same model setup for different sets of rheological parameters, and Figure 4 shows some variables resulting from a soft, medium and hard lithospheric strength.

[33] Initially, maximum compression (positive vertical strain rate on Figure 4d, dotted lines) is localized in front of the Indian plate indenter, for which the effective viscosity is always fixed at 10^{25} Pa s in all models. For a hard lithosphere (high viscosity), thickening is strongly localized near the indenter. At the beginning of the modeling (0 m.y.), the crust and lithosphere are homogeneous and of constant thickness, so there is no lateral variation of GPE and $\overline{\sigma}_{zz}$ is constant everywhere. In the center of the plateau GPE increases with the thickening of the crust and lithosphere, due to radiogenic heating and resulting decrease in mantle density, and after 65 m.y. of convergence the lateral variations of GPE are high enough to shift the locus of maximum lithospheric thickening northward away from the indentor (Figure 4d). For a medium or hard lithosphere, the lateral variations of GPE or $\overline{\sigma}_{zz}$ after 65 m.y. of convergence are not enough to prevail over the viscous forces, however; and the crustal and lithospheric thickness, and the surface elevation, all decrease continuously away from the indentor

Table 1. Parameters for Modeling[a]

Parameter	Value
Densities	
Crust and asthenosphere (ρ_c, ρ_a)	2800, 3200 kg m^{-3}
Lithospheric mantle	$\rho_m = \rho_a (1 + 1.75 \times 10^{-5} (T_{lit} - T_{moho}))$
T_{moho}, temperature at base of the crust	
Conductivities: crust, lithospheric mantle, asthenosphere	3.0, 3.2, 100.0 W m^{-1} K^{-1}
Heat production: crust, lithospheric mantle (z, depth in km)	2.5 exp(−z/15), 0 μW m^{-3}
If crustal thickness >40 km = >	2.5 exp(−z/55), 0 μW m^{-3}
Surface and bottom (z = 600 km) temperature	273, 1800 K
Base of the lithosphere, isotherm (T_{lit})	1300°C
Thermal diffusivity	1×10^{-6} m^2 s^{-1}
Rheology	
Crust: A [MPa^{-n} s^{-1}], n, Q [kJ mol^{-1}]	2.5×10^{-10}, 3, 100
Lithospheric mantle: A [MPa^{-n} s^{-1}], n, Q [kJ mol^{-1}]	4665, 3, 456
Dorn law: σ_D [Pa], Q_D [kJ mol^{-1}], $\dot{\varepsilon}_D$ [s^{-1}]	8.5×10^9, 500, 5.7×10^{11}
Model dimensions	4060 × 6020 km
Horizontal discretization grid (dx_1, dx_2)	35, 35 km

[a]See *Jiménez-Munt et al.* [2005a] for all the formulation.

with an approximately negative exponential form. The resulting orogen does not resemble the present-day Tibetan Plateau.

[34] Convergence in soft lithosphere with low viscosity, however, allows the deformation to diffuse more widely over the domain, reducing crustal thickening near the indenter and increasing it further north in the profile. The viscosity forces are not enough to sustain the orogen; with ~60 km of crustal thickness and ~3.9 km of elevation, the gravitational forces prevent further thickening in the central orogen and convergence is therefore accommodated further north. All the convergence migrates to the north and even some thinning is observed in the center of the orogen. As a result, the elevation and crustal thickness remain relatively constant for nearly 1000 km north of the indenter, producing a plateau, but the elevation at 3.9 km is significantly less than observed. The topographic gradient across the southern margin is steep, in agreement with observation, but on the northern margin the elevation decreases smoothly from 3.9 to 1 km, and the modeled elevation and crustal thickness (38 km) within Asia north of the plateau are much higher than observed.

[35] Note that significant softening of the orogen results from the increase in radiogenic heat production in the thickened crust. For a crustal thickness of 50 km and lithospheric mantle of 80 km, a decay exponent b = 55 for the decay of radiogenic heat production gives a Moho temperature ~280°C higher than if b = 15 km. This increase of the Moho temperature results in a reduction of the lithospheric strength by a factor of 5. The results for a soft lithosphere but without any increase in heat production with crustal thickness are also shown in Figure 4 (black dashed line). We can see a smoother pattern of deformation over the entire domain with no thinning on the plateau. In this model, as the heat production practically doesn't increase when crust is thicker than 40 km, there is no big temperature difference between the orogen and foreland. This, and the assumption of a soft lithosphere, results in a nearly constant Eurasian viscosity and therefore a much broader spread of deformation.

[36] The temperature at the base of the crust in all these models is always less than 700°C (Figure 4a). These values are low compared with observations: 700°C found between the upper and the middle crust under the southern Qiangtang block, 800°C at 32 km depth in the northern Lhasa block [*Mechie et al.*, 2004], 800°C to 900°C in the lower crust of the northern Tibetan Plateau [*Hacker et al.*, 2000], and Moho temperatures of 900–1100°C under the Qiangtang and 800–900°C beneath the Himalaya calculated by *Galvé et al.* [2006]. Therefore another process is needed to increase the temperature in the middle and lower crust.

5.1. Continuous Removal of Lithospheric Mantle

[37] We next consider the effect of continuous removal of lithospheric mantle during convergence, imposing a maximum depth of the base of the lithosphere (isotherm 1300°C), at 170 km (Figure 5). This is intended to simulate delamination or subduction of lithosphere during crustal thickening, as envisaged by *Tapponnier et al.* [2001], for example. The lithosphere is not allowed to get thicker than 170 km, and the methodology used is the same as that

Figure 4. Model results for indentation without any removal of lithospheric mantle. Plots show N-S profiles (located in Figure 3a) of model variables, from top to bottom: Moho temperature, gravitational potential energy changes, effective viscosity, vertical strain rate, elevation, crustal thickness and lithospheric mantle thickness. Each plot shows the initial stage (0 m.y.) for soft and hard rheologies (dotted lines), results after 65 m.y. of indentation at 50 mm yr^{-1} for soft, medium, and hard rheologies (continuous lines). Radiogenic heat production H = 2.5 exp(−z/15) μW m^{-3} when crust is thinner than 40 km and H = 2.5 exp(−z/55) μW m^{-3} when crust is thicker than 40 km. Dashed lines show results for a soft rheology without increasing heat production with crustal thickness.

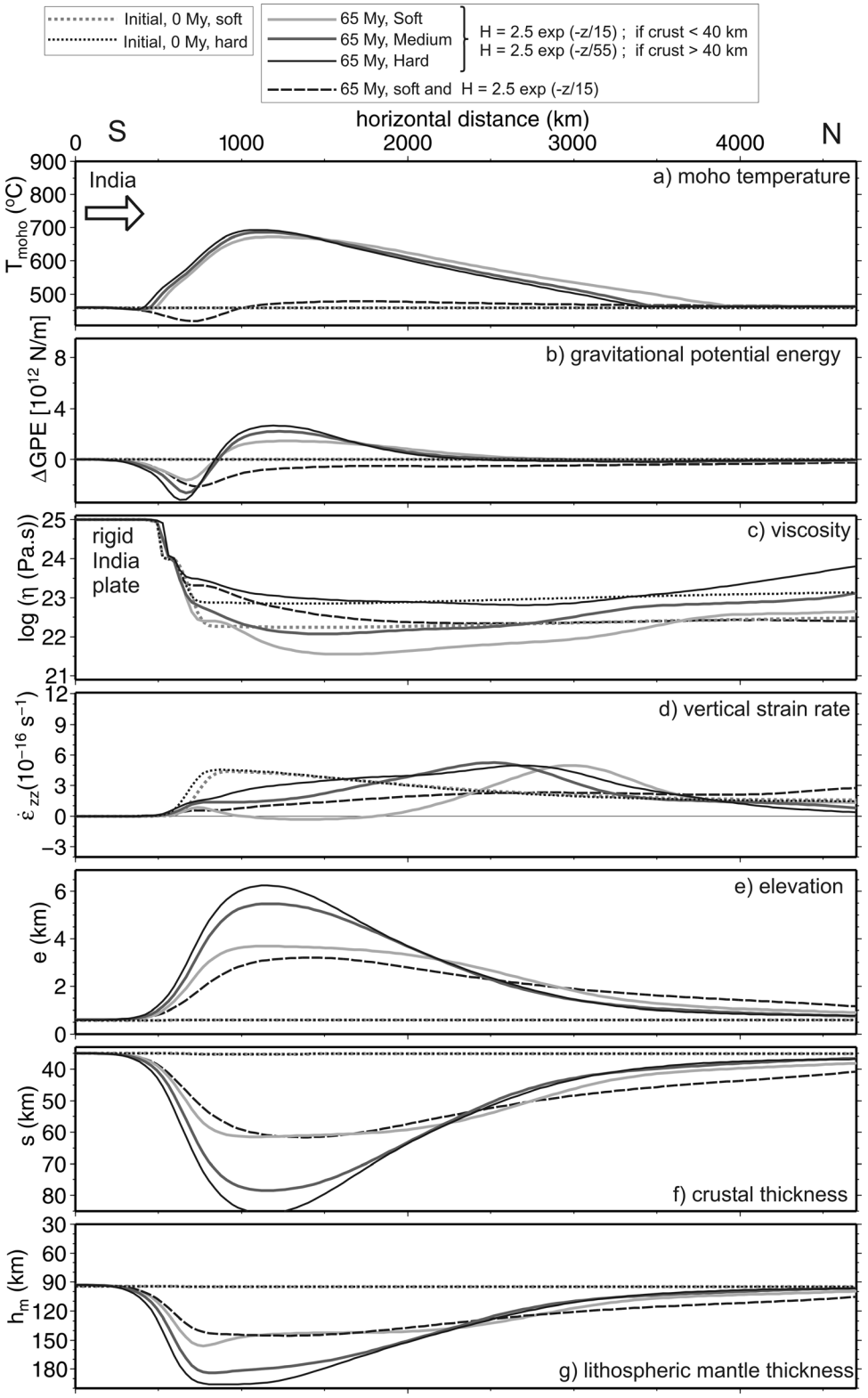
Initial, 0 My, soft
Initial, 0 My, hard
65 My, Soft
65 My, Medium
65 My, Hard
H = 2.5 exp (-z/15) ; if crust < 40 km
H = 2.5 exp (-z/55) ; if crust > 40 km
65 My, soft and H = 2.5 exp (-z/15)
horizontal distance (km)
0
S
1000
2000
3000
4000
N
India
a) moho temperature
T_{moho} (°C)
b) gravitational potential energy
ΔGPE [10^{12} N/m]
rigid India plate
c) viscosity
log (η (Pa.s))
d) vertical strain rate
$\dot{\varepsilon}_{zz}$(10^{-16} s^{-1})
e) elevation
e (km)
s (km)
f) crustal thickness
h_m (km)
g) lithospheric mantle thickness

Figure 4

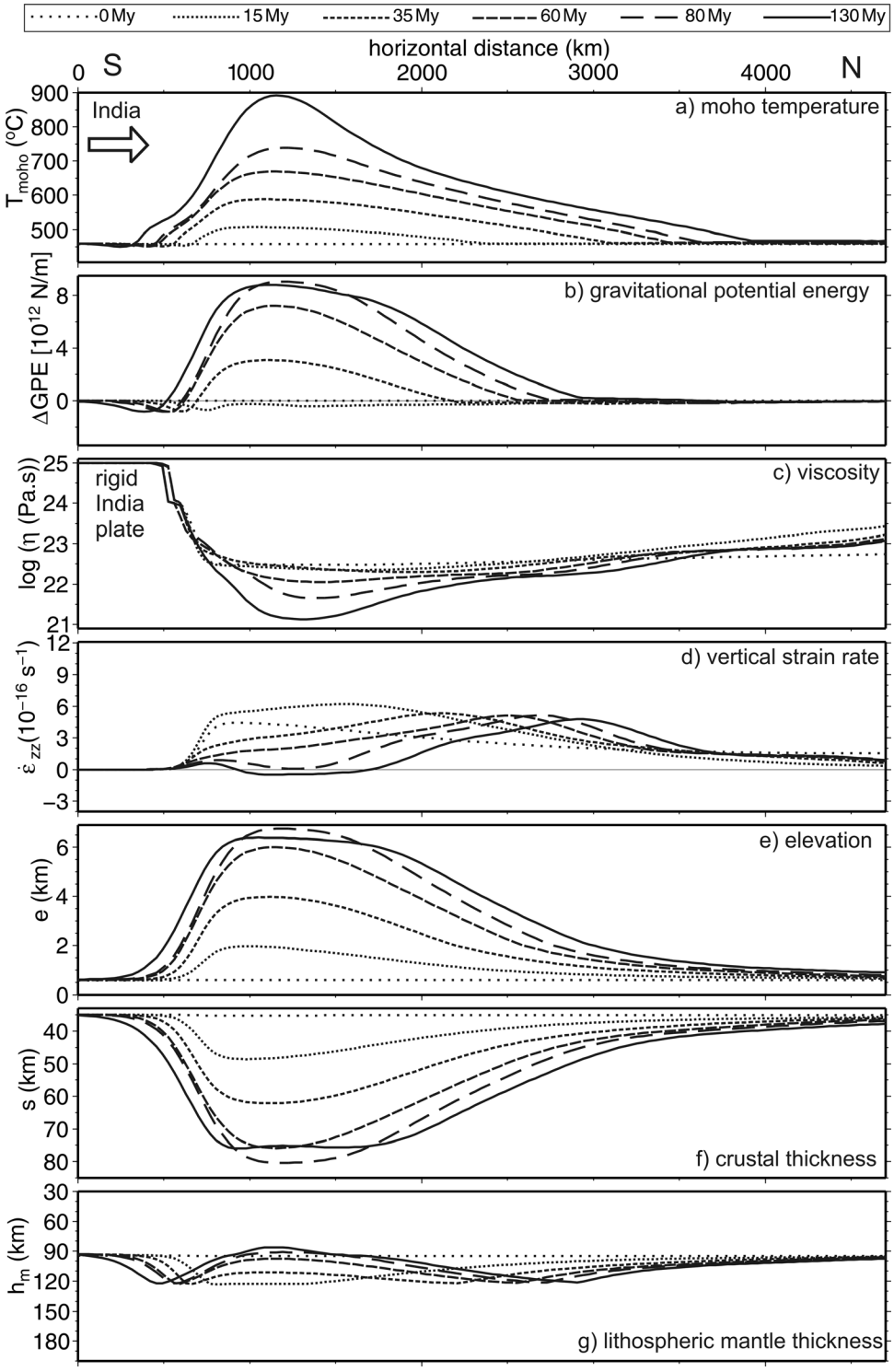

Figure 5. Model results for indentation with continuous removal of lithospheric mantle at 170 km depth. N-S profiles (located in Figure 3a) of model variables, from top to bottom: Moho temperature, gravitational potential energy changes, effective viscosity, vertical strain rate, elevation, crustal thickness and lithospheric mantle thickness. Results shown at 0, 15, 35, 60, 80, and 130 m.y. (from dotted to solid lines). Radiogenic heat production $H = 2.5 \exp(-z/15)$ μW m^{-3} when crust is thinner than 40 km and $H = 2.5 \exp(-z/55)$ μW m^{-3} when crust is thicker than 40 km.

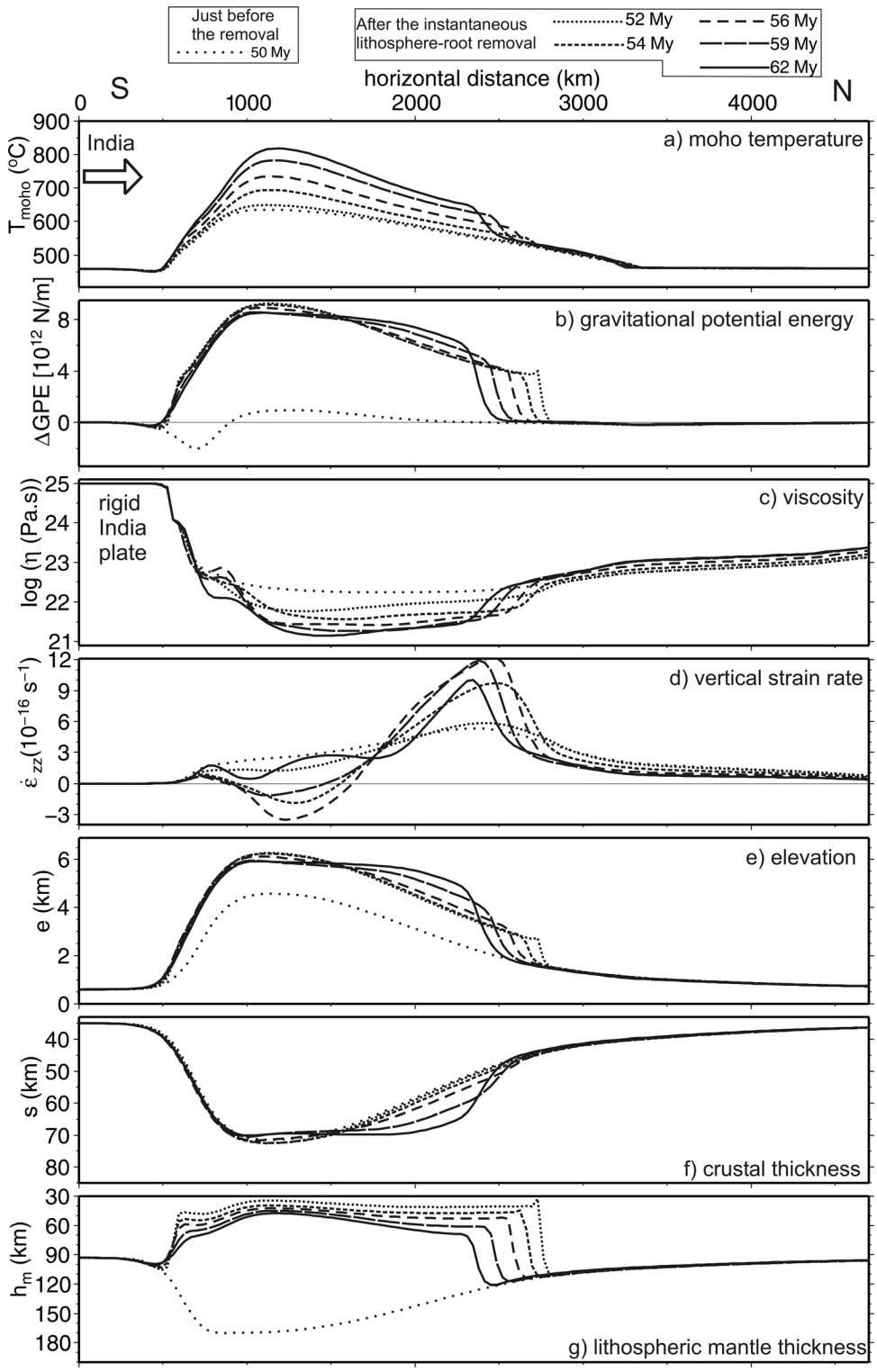

Figure 6. Model results for indentation with removal of lithospheric mantle at 50 m.y below the 700°C isotherm where thickness exceeds 155 km. N-S profiles (located in Figure 3a) of model variables, from top to bottom: Moho temperature, gravitational potential energy changes, effective viscosity, vertical strain rate, elevation, crustal thickness and lithospheric mantle thickness. Results shown before lithosphere removal (50 m.y.) and after removal (52, 54, 56, 59, 62 m.y.). Radiogenic heat production $H = 2.5 \exp(-z/15)$ μW m^{-3} and $H = 2.5 \exp(-z/55)$ μW m^{-3} when the crust is thicker than 40 km.

described for convective removal in the next section, applied during each time step in the areas where the 1300°C isotherm gets deeper than 170 km. As a result, the geotherm is not thickening at the same rate as the crust, and while the crust is thickening the lithospheric mantle can be thinning. In this sense, the crust and lithospheric mantle are partially decoupled.

[38] Under these conditions the lithosphere beneath the orogen reaches a maximum thickness of 170 km 12 m.y. after India-Asia collision (Figure 5). Figure 5 shows the time evolution of some variables along a S-N profile. The crust of the orogen is still getting thicker until 80 m.y., but the lithospheric mantle beneath it is being removed. Meanwhile, the GPE increases between the orogen and the foreland; but it is not sufficient to cause thinning of the highest areas of the orogen before 85 m.y. of convergence. The topographic profile up to this time therefore resembles that produced by whole lithosphere thickening, but with higher overall elevations (compare Figures 4 and 5). Only after about 85 m.y., thinning starts in the center of the orogen and the convergence is transmitted to the north of the plateau, where the rate of thickening reaches $\sim 5 \times 10^{-16}$ s^{-1}. As a result, after 130 m.y. of collision a flat plateau is produced that is ~1000 km wide, with an elevation of 6.5 km, and a crustal thickness of 75 km. At that time, the Moho temperature of the plateau has a maximum value at the center of 900°C, closer to the values suggested by *Galvé et al.* [2006].

[39] From this modeling, we see that assuming continuous removal of lithospheric mantle, the orogen would take about 130 m.y. to become at the same time flat and with some thinning in the center of the plateau. India-Eurasia collision started at 50–60 Ma. Figure 5 shows that within this time neither the observed elevation nor the flat plateau are well reproduced. Therefore another process is needed to accelerate the plateau formation.

5.2. Removal of the Lithosphere Root

[40] The next step was to study the influence of late stage removal of part of the lithospheric mantle under the thickened zones. We used the same model setup as in Figure 4, and up to 50 m.y. after the start of convergence the topography evolves in the same way as in Figure 4, with maximum elevation near the indentor and an approximately negative exponential decrease of surface elevation away from it. At 50 m.y. we assume instantaneous removal of the root where the lithosphere is thicker than 155 km, imposing the new base of the lithosphere at the 700°C isotherm. Modeling of the convective removal process by *Molnar et al.* [1998] suggests that material deeper than the 800°C isotherm could be removed, which corresponds to an

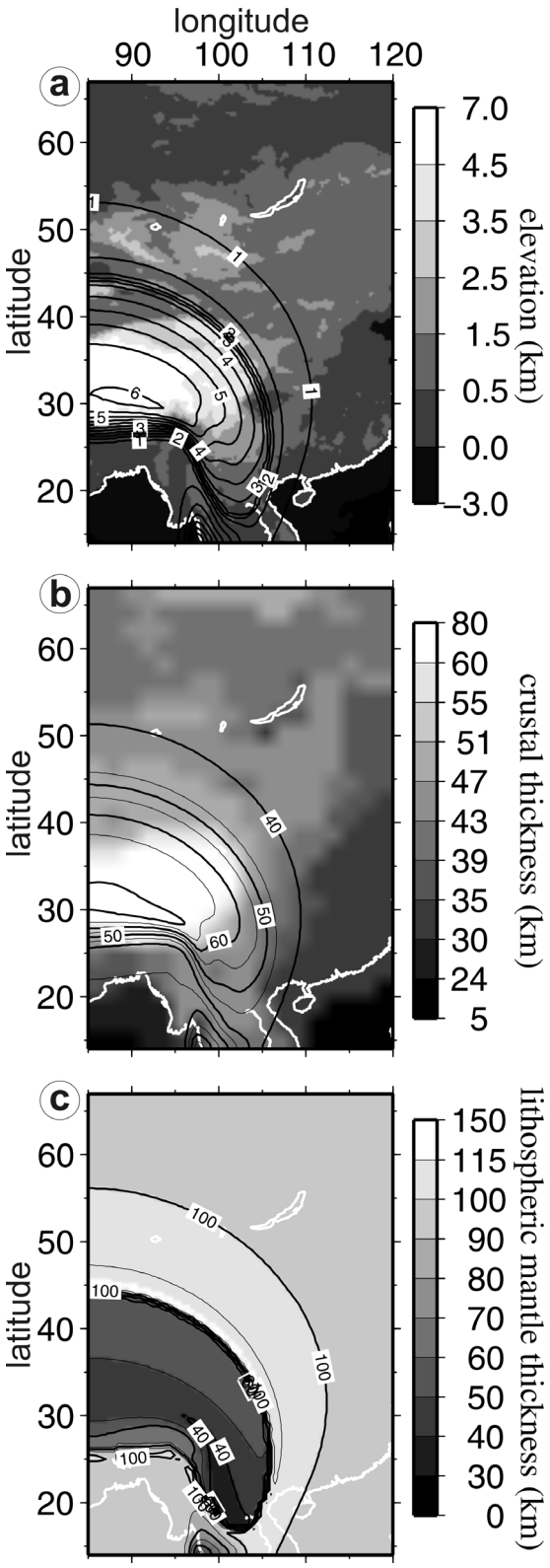

Figure 7. Model results after 57 m.y. of convergence at 50 mm yr^{-1} and 7 m.y. after removal of lithospheric mantle below the 700°C isotherm where thickness exceeds 155 km. Radiogenic heat production $H = 2.5 \exp(-z/15)$ μW m^{-3} and $H = 2.5 \exp(-z/55)$ μW m^{-3} if the crust is thicker than 40 km. (a) Elevation predicted from the model (contours) and measured (gray pattern); (b) crustal thickness predicted from the model (contours) and data (gray pattern, compiled by *Bassin et al.* [2000]); (c) lithospheric mantle thickness predicted from the model.

average thickness of ~125 km of mantle lithosphere. We assume a temperature 100°C lower for the controlling isotherm in order to achieve the observed surface elevation of the plateau.

[41] The lithospheric root is removed from an extended area about 2000 km from south to north (Figure 6g), leaving the lithospheric mantle thickness between 25 and 28 km in the center of the orogen and 40 km on its edges. This produces sharp increases in Moho temperature, surface elevation, and GPE in the region where the lithospheric root is removed (Figures 2 and 6). The warming of the lithosphere results in a decrease in its strength and viscosity, so that it is unable to sustain the increased lateral variation of GPE; as a result the convergence migrates to the north and some thinning takes place in the more elevated zones of the orogen (Figure 6d). After a further 5 m.y. this produces a relatively flat plateau with an elevation comparable to that of present-day Tibet.

[42] 10 m.y. after the instantaneous removal of the lithosphere root, thickening resumes over the whole orogen (positive vertical strain rate Figure 6d). This is due to the cooling and thickening of the lithospheric mantle and the thinning of the crust beneath the plateau, which lead to decreases in elevation and GPE. The fact that the crust beneath the Tibetan Plateau is currently undergoing tectonic thinning therefore suggests that removal of lithospheric mantle beneath Tibet occurred <9 m.y. ago, as proposed, for example, by *Molnar et al.* [1993].

[43] Note that the Indian convergence rate used here is the long-term average convergence rate of 50 mm yr^{-1} [*DeMets et al.*, 1994]. This is an approximation because the convergence rate varies along the Himalayan front and the rates changed in time [e.g., *Guillot et al.*, 2003; *Replumaz and Tapponnier*, 2003]. Recent GPS data indicate rates of 35 mm yr^{-1} [*Paul et al.*, 2001]. If we use 35 mm yr^{-1} for the India convergence rate after lithospheric removal, we predict that normal faulting and thinning on the plateau will continue up to 12 m.y. after removal of the lithosphere root, but not later on. This prediction is in broad agreement with those studies that indicate removal of lithospheric mantle, plateau uplift, and the onset of normal faulting in the middle to late Miocene [e.g., *Blisniuk et al.*, 2001; *Clark et al.*, 2005; *Hou et al.*, 2004; *Turner et al.*, 1996; *Sun et al.*, 2005; *Wang et al.*, 2006].

[44] The viscosities predicted from the model (Figure 6c) are between 2 and 10×10^{21} Pa s on the plateau and $3-7 \times 10^{23}$ Pa s on the foreland, in agreement with the effective viscosity inferred by *Flesch et al.* [2001] from Quaternary fault slip rates and GPS velocities.

[45] Figure 7 shows in plan view the elevation and crustal and lithospheric mantle thicknesses after 57 m.y. of convergence and 7 m.y. after removal of the lithosphere root. The maximum elevation is 6 km, but a large area, nearly 10° from south to north, is at the same elevation ~5.5 km. The crustal thickness beneath the flat area is between 65 and 70 km, decreasing to the north and east to ~37 km. These regional values are in agreement with the measured crustal thickness (gray pattern in Figure 7b, data compiled by *Bassin et al.* [2000]). The lithospheric mantle is clearly thinner under the plateau, with values between 40 and 50 km; it reaches 115 km on the edges of the plateau, and then decreases to 90–100 km beneath the Asia foreland and the Indian plate.

[46] The horizontal velocity field and the principal components of the horizontal stress tensor are shown in Figure 8. The plateau has three main areas. On the southern front, near the contact with the Indian indenter, there is a narrow band where the main deformation is by thrusting with positive component of the vertical strain rate (or thickening). In the center of the high plateau the deformation is by normal faulting or transtension, with the maximum extension direction oriented nearly E-W. On the northern flank of the plateau there is thickening with high positive values of the vertical strain rate, and the principal horizontal compressive stress is NE-SW or NNE-SSW. The predicted pattern of crustal thickening and thinning (Figure 8a) is comparable to that obtained by *Holt et al.* [2000] from GPS observations and Quaternary fault slip rates. Our model predicts thinning values between 2 and 10×10^{-16} s^{-1} in the center of the plateau, and somewhat higher values of 10×10^{-16} s^{-1} of thickening on the northern flank, in agreement with *Holt et al.* [2000]. The high rate of thickening ($20-30 \times 10^{-16}$ s^{-1}) obtained by *Holt et al.* [2000] on the Himalayan front is not reproduced by our numerical modeling, as the thin viscous sheet method doesn't permit modeling of the discontinuity itself; our values on the India-Tibet contact are $\sim 1 \times 10^{-16}$ s^{-1}.

[47] The horizontal stress directions in Figure 8b reproduce the main features from the observations compiled on the World Stress Map [*Reinecker et al.*, 2005]. In the center of the plateau the maximum tensional deviatoric stress is E-W and normal faulting is the predominant tectonic regime. On the eastern and northeastern plateau the principal stress direction rotates clockwise, increasing the compressional component and decreasing the extensional. On the margins of the plateau the main tectonic regime is reverse faulting with the compressive axis following the steepest topography gradient. This is also in agreement with the correlation

Figure 8. Model results after 57 m.y. of convergence at 50 mm yr^{-1} and 7 m.y. after removal of lithospheric mantle below the 700°C isotherm where thickness exceeds 155 km. Radiogenic heat production $H = 2.5 \exp(-z/15)$ μW m^{-3} and $H = 2.5 \exp(-z/55)$ μW m^{-3} if the crust is thicker than 40 km. (a) Horizontal velocity field (arrows), vertical strain rate (color pattern, positive for thickening and negative for thinning) and crustal thickness (contours every 10 km). Gray outline is the region of the plots on Figures 8b and 8c. (b) Horizontal principal stress directions (arrows for extension and bars for compression), tectonic regime (color pattern) and elevation (contours every 0.5 km). Note that this plot is a zoom on the plateau (gray outline Figure 8a). (c) Vorticity (color pattern in rad sv), vertical axis finite rotations (circled numbers in degrees), and elevation (contours in km). This plot is also a zoom on the plateau (gray outline Figure 8a).

between elevation and tectonic regime shown by *Molnar et al.* [1993].

[48] We can compare the predicted velocity field (Figure 8a) with that from GPS measurements (Figure 1). The velocity field on the plateau rotates clockwise toward the east, and on the eastern side of the plateau the horizontal velocity is E-W directed. We can also observe this clockwise rotation from the present vorticity and the accumulated

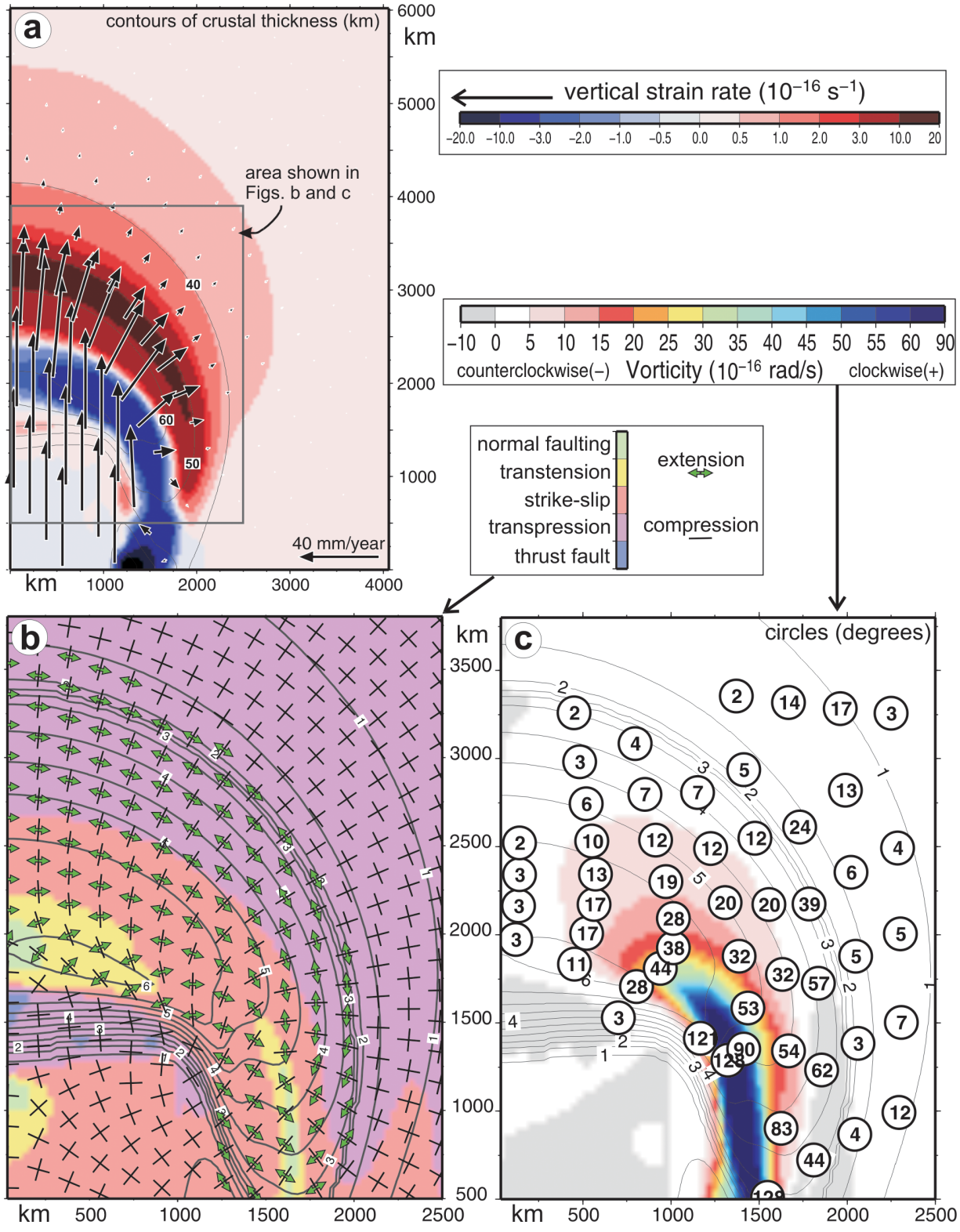

Figure 8

vertical axis rotation during the 57 m.y. period (Figure 8c). The finite rotation θ is obtained by integrating with time half of the vertical component of the vorticity of the flow [*Jiménez-Munt et al.*, 2005b],

$$\theta = \frac{1}{2}\int (\text{vorticity})dt,$$

where

$$\text{vorticity} = \frac{\partial u_2}{\partial x_1} - \frac{\partial u_1}{\partial x_2},$$

u_1 and u_2 are the horizontal components of the velocity in x_1 and x_2 directions, and t is time.

[49] Our predicted vorticity is directly comparable with the present rotation rate from *Holt et al.* [2000]. The highest clockwise rotation is on the eastern contact between the Indian indenter and the Asian plate, with maximum values of 50 and 80 rad s^{-1}; and north of the Tibetan Plateau the rotation is mainly counterclockwise.

6. Conclusions

[50] Our modeling results suggest that in order to reproduce the present topography of the Tibetan Plateau, with east-west extension and crustal thinning as the dominant current active deformation, two processes are required in addition to lithospheric thickening.

[51] 1. Dense lithospheric mantle material must have been removed from beneath Tibet in order to explain the present surface elevation and lack of regional surface slope. In the absence of this removal, the modeled topography for Tibet has a maximum elevation of <4000 m (for weak rheology), or the surface slopes significantly northward, away from the Indian indentor (for strong rheology).

[52] 2. The middle and lower crust must have been warmed and weakened by an increase in depth of radiogenic heat production at depth due to the duplication of the crust. Weakening of the Tibetan crust by conductive warming would require tens of millions of years [*Shapiro et al.*, 2004], therefore other processes such as increased mantle heat flow consequent upon the removal of lithospheric mantle, and advective transport of heat by magma may have to be involved. In the absence of this warming and weakening, viscous stresses associated with plate convergence would exceed stresses produced by the surface elevation, and the present pattern of vertical thinning and east-west extension would not have developed.

[53] Continuous removal of lithosphere, by delamination or convection, does not produce sufficient warming and weakening of the lower crust, and fails to reproduce either the present topography or the pattern of active deformation on the plateau in a reasonable time. A much longer period of convergence would be needed in order to reproduce the present characteristics of the plateau.

[54] Geologically rapid removal of the lithospheric root beneath the thickened crust of Tibet also successfully explains the current elevation of the plateau, its lack of surface slope, the steep south and north margins, and the pattern of the present deformation, including vertical thinning, E-W extension, and extrusion and vertical axis rotation on the eastern margin. Our modeling suggests that this removal took place within the last 12 m.y.

[55] The agreement between model results and observations could be greatly improved by adding additional complexity and parameters to the model assumptions, for example by introducing stronger and weaker areas within the foreland, individual faults, or decoupled upper and lower crust. However, our results indicate that on a regional scale the large-scale structure, evolution, topography and strain rate distribution, can be understood as a result of the convergence between India and Eurasia acting on a rheologically layered crust–lithospheric mantle system. Our results are also consistent with the present-day N-S variations of the properties of the lithosphere.

[56] **Acknowledgments.** I. Jiménez-Munt was supported by the Spanish Government by the Program "Ramón y Cajal." The authors thank the Group of Dynamics of the Lithosphere from CSIC-Barcelona and A. Galvé and A.M. Negredo for enlightening discussions. Constructive reviews from C. Beaumont and R. Pysklywec, and the advice of the Associate Editor L. Ratschbacher, helped us improve the final version.

References

Achache, J., V. Courtillot, and Y. X. Zhou (1984), Paleogeographic and tectonic evolution of southern Tibet since middle Cretaceous time: New paleomagnetic data and synthesis, *J. Geophys. Res.*, *89*, 10,311–10,339.

Alsdorf, D., L. Brown, K. D. Nelson, Y. Makovsky, S. Klemperer, and W. Zhao (1998), Crustal deformation of the Lhasa terrane, Tibet Plateau from Project INDEPTH deep seismic reflection profiles, *Tectonics*, *17*, 501–519.

Avouac, J.-P., and P. Tapponnier (1993), Kinematic model of active deformation in central Asia, *Geophys. Res. Lett.*, *20*, 895–898.

Bassin, C., G. Laske, and G. Masters (2000), The Current Limits of Resolution for Surface Wave Tomography in North America, *Eos Trans. AGU*, *81*(48), Fall Meet. Suppl., Abstract S12A-03.

Beaumont, C., R. A. Jamieson, M. H. Nguyen, and B. Lee (2001), Himalayan tectonics explained by extrusion of a low-viscosity crustal channel coupled to focused surface denudation, *Nature*, *414*, 738–742.

Bird, P. (1989), New finite element techniques for modeling deformation histories of continents with stratified temperature-dependent rheology, *J. Geophys. Res.*, *94*, 3967–3990.

Bird, P. (1991), Lateral extrusion of lower crust from under high topography, in the isostatic limit, *J. Geophys. Res.*, *96*, 10,275–10,286.

Blisniuk, P. M., B. R. Hacker, J. Glodny, L. Ratschbacher, S. Bi, Z. Wu, M. O. McWilliams, and A. Calvert (2001), Normal faulting in central Tibet since at least 13.5 Myr ago, *Nature*, *412*, 628–632.

Chen, W.-P., and P. Molnar (1983), Focal depths of intracontinental and intraplate earthquakes and their implications for the thermal and mechanical properties of the lithosphere, *J. Geophys. Res.*, *88*, 4183–4214.

Chung, S.-L., C.-H. Lo, T.-Y. Lee, Y. Zhang, Y. Xie, X. Li, K.-L. Wang, and P.-L. Wang (1998), Diachronous uplift of the Tibetan Plateau starting 40 Myr ago, *Nature*, *394*, 769–773.

Chung, S.-L., D. Liu, J. Ji, M.-F. Chu, H.-Y. Lee, D.-J. Wen, C.-H. Lo, T.-Y. Lee, Q. Qian, and Z. Qi (2003), Adakites from continental collision zones: Melting of thickened lower crust beneath southern Tibet, *Geology*, *31*, 1021–1024.

Clark, M. K., and L. H. Royden (2000), Topographic ooze: Building the eastern margin of Tibet by lower crustal flow, *Geology*, *28*, 703–706.

Clark, M. K., M. A. House, L. H. Royden, K. X. Whipple, B. C. Burchfiel, X. Zhang, and W. Tang (2005), Late Cenozoic uplift of southeastern Tibet, *Geology*, *33*, 525–528.

Coleman, M. E., and K. V. Hodges (1995), Evidence for Tibetan Plateau uplift before 14 Myr ago from a new minimum estimate for east-west extension, *Nature*, *474*, 49–52.

DeMets, C., R. G. Gordon, D. F. Argus, and S. Stein (1994), Effect of recent revisions to the geomag-

netic reversal time scale on estimates of current plate motions, *Geophys. Res. Lett.*, *21*, 2191–2194.
Dewey, J. F., R. M. Shackleton, C. Chengfa, and S. Yiyin (1988), The tectonic evolution of the Tibetan Plateau, *Philos. Trans. R. Soc. London, Ser. A*, *327*, 379–413.
England, P. C., and G. A. Houseman (1986), Finite strain calculations of continental deformation. 2. Comparison with the India-Asia collision zone, *J. Geophys. Res.*, *91*, 3664–3676.
England, P. C., and G. A. Houseman (1989), Extension during continental convergence, with application to the Tibetan Plateau, *J. Geophys. Res.*, *94*, 17,561–17,579.
England, P. C., and P. Molnar (1997), Active deformation of Asia: From kinematics to dynamics, *Science*, *278*, 647–650.
England, P. C., and M. P. Searle (1986), The Cretaceous-Tertiary deformation of the Lhasa block and its implications for the crust al thickening of Tibet, *Tectonics*, *5*, 1–14.
Fielding, E., B. Isacks, M. Barazangi, and C. Duncan (1994), How flat is Tibet?, *Geology*, *22*, 163–167.
Flesch, L. M., A. J. Haines, and W. E. Holt (2001), Dynamics of the India-Eurasia collision zone, *J. Geophys. Res.*, *106*, 16,435–16,460.
Galvé, A., M. Jiang, A. Hirn, M. Sapin, M. Laigle, B. de Voogd, J. Gallart, and H. Qian (2006), Explosion seismic P and S velocity and attenuation constraints on the lower crust of the North-Central Tibetan Plateau, and comparison with the Tethyan Himalayas: Implications on composition, mineralogy, temperature, and tectonic evolution, *Tectonophysics*, *412*, 141–157.
Griot, D.-A., J.-P. Montagner, and P. Tapponnier (1998), Phase velocity structure from Rayleigh and Love waves in Tibet and its neighboring regions, *J. Geophys. Res.*, *103*, 21,215–21,232.
Guillot, S., E. Garzanti, D. Baratoux, D. Marquer, G. Mahéo, and J. de Sigoyer (2003), Reconstructing the total shortening history of the NW Himalaya, *Geochem. Geophys. Geosyst.*, *4*(7), 1064, doi:10.1029/2002GC000484.
Hacker, B. R., E. Gnos, L. Ratschbacher, M. Grove, M. McWilliams, S. V. Sobolev, J. Wan, and W. Zhenhan (2000), Hot and dry deep crustal xenoliths from Tibet, *Science*, *287*, 2463–2466.
Haines, S. S., S. L. Klemperer, L. Brown, J. Guo, J. Mechie, R. Meissner, A. Ross, and W. Zhao (2003), INDEPTH III seismic data: From surface observations to deep crustal processes in Tibet, *Tectonics*, *22*(1), 1001, doi:10.1029/2001TC001305.
Hauck, M. L., K. D. Nelson, L. D. Brown, W. Zhao, and A. R. Ross (1998), Crustal structure of the Himalayan orogen at ~90° east longitude from Project INDEPTH deep reflection profiles, *Tectonics*, *17*, 481–500.
Hodges, K. V. (2000), Tectonics of the Himalaya and southern Tibet from two perspectives, *Geol. Soc. Am. Bull.*, *112*, 324–350.
Holt, W. E., N. Chamot-Rooke, X. Le Pichon, A. J. Haines, B. Shen-Tu, and J. Ren (2000), Velocity field in Asia inferred from Quaternary fault slip rates and Global Positioning System observations, *J. Geophys. Res.*, *105*, 19,185–19,209.
Hou, Z.-Q., Y.-F. Gao, X.-M. Qu, Z.-Y. Rui, and X.-X. Mo (2004), Origin of adakitic intrusives generated during mid-Miocene east-west extension in the southern Tibet, *Earth Planet. Sci. Lett.*, *220*, 139–155.
Houseman, G. A., and P. England (1986), Finite strain calculations of continental deformation: 1. Method and general results for convergent zones, *J. Geophys. Res.*, *91*, 3651–3663.
Houseman, G. A., and P. Molnar (2001), Mechanisms of lithospheric rejuvenation associated with continental orogeny, in *Continental Reactivation and Reworking*, edited by J. A. Miller et al., *Geol. Soc. Spec. Publ.*, *184*, 13–38.
Houseman, G. A., D. P. McKenzie, and P. Molnar (1981), Convective instability of a thickened boundary layer and its relevance for the thermal evolution of continental convergence belts, *J. Geophys. Res.*, *86*, 6115–6132.
Jiménez-Munt, I., M. Fernàndez, M. Torne, and P. Bird (2001), The transition from linear to diffuse plate boundary in the Azores-Gibraltar region: Results from a thin sheet model, *Earth Planet. Sci. Lett.*, *192*, 175–189.
Jiménez-Munt, I., D. Garcia-Castellanos, and M. Fernàndez (2005a), Thin-sheet modelling of lithospheric deformation and surface mass transport, *Tectonophysics*, *407*, 239–255.
Jiménez-Munt, I., D. Garcia-Castellanos, A. M. Negredo, and J. P. Platt (2005b), Gravitational and tectonic forces controlling postcollisional deformation and the present-day stress field of the Alps: Constraints from numerical modeling, *Tectonics*, *24*, TC5009, doi:10.1029/2004TC001754.
Jin, Y., M. K. McNutt, and Y. Zhu (1994), Evidence from gravity and topography data for folding of Tibet, *Nature*, *371*, 669–674.
Kapp, P., and J. H. Guynn (2004), Indian punch rifts Tibet, *Geology*, *32*, 993–996.
Liu, M., and Y. Yang (2003), Extensional collapse of the Tibetan Plateau: Results of three-dimensional finite element modeling, *J. Geophys. Res.*, *108*(B8), 2361, doi:10.1029/2002JB002248.
McNamara, D., W. Walter, T. Owens, and C. Ammon (1997), Upper mantle velocity structure beneath the Tibetan Plateau from Pn travel time tomography, *J. Geophys. Res.*, *102*, 493–505.
Mechie, J., S. V. Sobolev, L. Ratschbacher, A. Y. Babeyko, G. Bock, A. G. Jones, K. D. Nelson, K. D. Solon, L. D. Brown, and W. Zhao (2004), Precise temperature estimation in the Tibetan crust from seismic detection of the α-β quartz transition, *Geology*, *32*, 601–604.
Molnar, P. M., and H. Lyon-Caen (1989), Fault plane solutions of earthquakes and active tectonics of the Tibetan Plateau and its margins, *Geophys. J. Int.*, *99*, 123–153.
Molnar, P., and P. Tapponnier (1977), Relation of the tectonics of eastern China to the Indo-Eurasian collision: Application of slip line field theory to large-scale continental tectonics, *Geology*, *5*, 212–216.
Molnar, P., P. C. England, and J. Martinod (1993), Mantle dynamics, uplift of the Tibetan Plateau, and the Indian monsoon, *Rev. Geophys.*, *31*, 357–396.
Molnar, P., G. A. Houseman, and C. P. Conrad (1998), Rayleigh-Taylor instability and convective thinning of mechanically thickened lithosphere: Effects of non-linear viscosity decreasing exponentially with depth and of horizontal shortening of the layer, *Geophys. J. Int.*, *133*, 568–584.
Murphy, M. A., A. Yin, T. M. Harrison, S. B. Dür, Z. Chen, F. J. Ryerson, W. S. F. Kidd, X. Wang, and X. Zhou (1997), Did the Indo-Asian collision alone create the Tibetan Plateau?, *Geology*, *25*, 719–722.
Neil, E. A., and G. A. Houseman (1997), Geodynamics of the Tarim Basin and the Tian Shan in central Asia, *Tectonics*, *16*, 571–584.
Parsons, B., and D. Mckenzie (1978), Mantle convection and the thermal structure of the plates, *J. Geophys. Res.*, *83*, 4485–4496.
Paul, J., et al. (2001), The motion and active deformation of India, *Geophys. Res. Lett.*, *28*, 647–650.
Platt, J. P., and P. England (1994), Convective removal of lithosphere beneath mountain belts: Thermal and mechanical consequences, *Am. J. Sci.*, *294*, 307–336.
Reinecker, J., O. Heidbach, M. Tingay, B. Sperner, and B. Müller (2005), The release 2005 of the World Stress Map, Geophys. Inst., Karlsruhe Univ., Karlsruhe, Germany. (Available at http://www.world-stress-map.org)
Replumaz, A., and P. Tapponnier (2003), Reconstruction of the deformed collision zone between India and Asia by backward motion of lithospheric blocks, *J. Geophys. Res.*, *108*(B6), 2285, doi:10.1029/2001JB000661.
Rowley, D. B., and B. S. Currie (2006), Palaeo-altimetry of the late Eocene to Miocene Lunpola basin, central Tibet, *Nature*, *439*, 677–681.
Searle, M. P., et al. (1987), The closing of Tethys and the tectonics of the Himalaya, *Geol. Soc. Am. Bull.*, *98*, 678–701.
Shapiro, N. M., M. H. Ritzwoller, P. Molnar, and V. Levin (2004), Thinning and flow of Tibetan crust constrained by seismic anisotropy, *Science*, *305*, 233–236.
Shen, F., L. H. Royden, and B. Clark Burchfiel (2001), Large-scale crustal deformation of the Tibetan Plateau, *J. Geophys. Res.*, *106*, 6793–6816.
Shi, D., et al. (2004), Detection of southward intracontinental subduction of Tibetan lithosphere along the Bangong-Nujiang suture by P-to-S converted waves, *Geology*, *32*, 209–212.
Spicer, R. A., N. W. B. Harris, M. Widdowson, A. B. Herman, S. Guo, P. J. Valdes, J. A. Wolfe, and S. P. Kelley (2003), Constant elevation of southern Tibet over the past 15 million years, *Nature*, *421*, 622–624.
Sun, J., R. Zhu, and Z. An (2005), Tectonic uplift in the northern Tibetan Plateau since 13.7 Ma ago inferred from molasses deposits along the Altyn Tagh Fault, *Earth Planet. Sci. Lett.*, *235*, 641–653.
Tapponnier, P., Z. Xu, F. Roger, B. Meyer, N. Arnaud, G. Wittlinger, and J. Yang (2001), Oblique stepwise rise and growth of the Tibet Plateau, *Science*, *294*, 1671–1677, doi:10.1126/science.105978.
Taylor, M., A. Yin, F. J. Ryerson, P. Kapp, and L. Ding (2003), Conjugate strike-slip faulting along the Bangong-Nujiang suture zone accommodates coeval east-west extension and north-south shortening in the interior of the Tibetan Plateau, *Tectonics*, *22*(4), 1044, doi:10.1029/2002TC001361.
Tilmann, F., J. Ni, and INDEPTH III Seismic Team (2003), Seismic imaging of the downwelling Indian lithosphere beneath central Tibet, *Science*, *300*, 1424–1427, doi:10.1126/science.1082777.
Turner, S., N. Arnaud, J. Liu, N. Rogers, C. Hawkesworth, N. Harris, S. Kelley, P. van Calsteren, and W. Deng (1996), Post-collision, shoshonitic volcanism in the Tibetan Plateau: Implications for convective thinning of the lithosphere and the source of ocean island basalts, *J. Petrol.*, *37*, 45–71.
Wang, Q., et al. (2001), Present-day crustal deformation in China constrained by Global Positioning System measurements, *Science*, *294*, 574–577, doi:10.1126/science.1063647.
Wang, Y., T. Deng, and D. Biasatti (2006), Ancient diets indicate significant uplift of southern Tibet after ca. 7 Ma, *Geology*, *34*, 309–312, doi:10.1130/G22254.1.
Williams, H., S. Turner, S. Kelley, and N. Harris (2001), Age and composition of dikes in southern Tibet: New constraints on the timing of east-west extension and its relationship to postcollisional volcanism, *Geology*, *29*, 339–342.
Wollenberg, H. A., and A. R. Smith (1987), Radiogenic heat production of crustal rocks: An assessment based on geochemical data, *Geophys. Res. Lett.*, *14*, 295–298.
Yin, A. (2000), Mode of Cenozoic east-west extension in Tibet suggesting a common origin of rifts in Asia during the Indo-Asian collision, *J. Geophys. Res.*, *105*, 21,745–21,759.
Yin, A., and T. M. Harrison (2000), Geologic evolution of the Himalayan-Tibetan orogen, *Annu. Rev. Earth Planet. Sci.*, *28*, 211–280.

I. Jiménez-Munt, Group of Dynamics of the Lithosphere, Institute of Earth Sciences "Jaume Almera," CSIC, Lluís Solé i Sabarís s/n, E-08028 Barcelona, Spain. (ivone@ija.csic.es)

J. P. Platt, Department of Earth Sciences, University of Southern California, Los Angeles, CA 90089-0740, USA. (jplatt@usc.edu)